

Distributional Reinforcement Learning with Diffusion Bridge Critics

Shutong Ding^{1,2*} Yimiao Zhou^{1,2*} Ke Hu^{1,2} Mokai Pan^{1,2} Shan Zhong³
 Yanwei Fu⁴ Jingya Wang^{1,2} Ye Shi^{1,2†}

Abstract

Recent advances in diffusion-based reinforcement learning (RL) methods have demonstrated promising results in a wide range of continuous control tasks. However, existing works in this field focus on the application of diffusion policies while leaving the diffusion critics unexplored. In fact, since policy optimization fundamentally relies on the critic, accurate value estimation is far more important than the policy expressiveness. Furthermore, given the stochasticity of most reinforcement learning tasks, it has been confirmed that the critic is more appropriately depicted with a distributional model. Motivated by these points, we propose a novel distributional RL method with Diffusion Bridge Critics (DBC). DBC directly models the inverse cumulative distribution function (CDF) of the Q value. This allows us to accurately capture the value distribution and prevents it from collapsing into a trivial Gaussian distribution owing to the strong distribution-matching capability of the diffusion bridge. Moreover, we further derive an analytic integral formula to address discretization errors in DBC, which is essential in value estimation. To our knowledge, DBC is the first work to employ the diffusion bridge model as the critic. Notably, DBC is also a plug-and-play component and can be integrated into most existing RL frameworks. Experimental results on MuJoCo robot control benchmarks demonstrate the superiority of DBC compared with previous distributional critic models.

1. Introduction

Diffusion models have recently been applied to reinforcement learning and demonstrate their superior performance in robot locomotion control and manipulation tasks (Ren

¹ShanghaiTech University ²InstAdapt ³University of Electronic Science and Technology of China ⁴Fudan University. Correspondence to: Ye Shi <shiyeye@shanghaitech.edu.cn>.

et al., 2024; Yang et al., 2023; Janner et al., 2022; Wang et al., 2022; Ajay et al., 2022; Chi et al., 2023) for their multimodality and powerful exploration capability. However, existing diffusion-based RL methods (Yang et al., 2023; Ding et al., 2024; 2025; Celik et al., 2025; Wang et al., 2024b; Psenka et al., 2023) principally focus on leveraging diffusion models to enhance the policy expressiveness, while overlooking the potential of diffusion on modeling the distributional critic. In fact, the critic plays a more important role in RL, as policy optimization are driven by the values or gradients estimated by the critic model.

Distributional critics (Bellemare et al., 2017) were originally proposed to better capture the inherent stochasticity in RL, thereby yielding more accurate value estimates for policy training. The core idea of existing works (Kuznetsov et al., 2020; Dabney et al., 2018b) in this area is to represent the Q-value distribution using finite discrete quantiles to approximate the Q-values at each quantile with neural networks. Although these methods can improve Q-value estimation to some extent, it remains restricted by the discrete quantile representation and the limited expressiveness of neural networks. Besides, recent works such as (Hu et al., 2025; Zhong et al., 2025a) also attempt to apply diffusion models to depict the Q-value distribution for its expressiveness. However, under the diffusion learning paradigm, the Bellman backup operator induces an unbounded accumulation of approximation errors, causing the diffusion critic to eventually collapse into a trivial Gaussian distribution.

To overcome these issues and obtain more accurate value estimation, we propose Diffusion Bridge Critics (DBC), a novel distributional RL method that leverages expressive diffusion bridge models to depict the Q-value distribution. Concretely, DBC learns the inverse cumulative distribution function (inverse CDF) of the Q-value distribution. This formulation aligns naturally with quantile-based distributional reinforcement learning, while avoiding discrete quantile approximations and the Gaussian degradation problem in vanilla diffusion critics. Besides, we also find that a key technical challenge in diffusion bridges for policy optimization lies in discretization errors arising from finite-time approximations. To address this challenge, we derive an analytic integral form that corrects the bias induced by discrete diffusion steps, resulting in more accurate value estimation

and stable policy improvement. Notably, DBC is a plug-and-play approach, which can be seamlessly integrated into existing RL algorithms without modifying the underlying policy architecture or optimization procedure. To summarize, our contribution is threefold:

- **Gaussian Degradation of Vanilla Diffusion Critic.** We identify and analyze the issue of directly employing diffusion models as critics in reinforcement learning, which leads to the degradation of itself to trivial Gaussian distributions with the Bellman backup operator. Consequently, it severely limits the expressiveness of the learned value distribution and undermines effective policy optimization.
- **Diffusion Bridge as Distributional Critic.** We propose Diffusion Bridge Critics (DBC), a novel distributional RL method that employs diffusion bridge models to accurately learn the inverse cumulative distribution function (CDF) of the Q-value distribution. With the anchor loss design and integral-consistent discretization technique, DBC is the first success that effectively incorporates diffusion bridge critics into distributional RL.
- **State-of-the-art Performance.** We evaluate DBC combined with SAC and TD3 on a range of MuJoCo robotic control tasks and compare it with other representative distributional RL methods. Results demonstrate that DBC consistently achieves state-of-the-art performance, validating the effectiveness of diffusion bridge critics and highlighting the importance of an expressive diffusion-based critic in reinforcement learning.

2. Related Works

Diffusion-based Reinforcement Learning. Existing diffusion-based RL methods mostly focus on the technique of diffusion policy optimization. In offline RL, diffusion models (Janner et al., 2022; Wang et al., 2022; Ajay et al., 2022) are employed to approximate the behavior policy in the offline dataset and enable policy optimization by sampling actions or trajectories that remain within the support of the diffusion model. In off-policy reinforcement learning, DIPO (Yang et al., 2023) and QSM (Psenka et al., 2023) optimize the diffusion policy by utilizing the gradient of the Q function. DACER (Wang et al., 2024b) and DIME (Celik et al., 2025) treat the diffusion policy as a black-box model and directly apply deterministic policy gradient with different techniques on entropy estimation. Besides, QVPO (Ding et al., 2024), (SDAC) (Ma et al., 2025a) perform the policy improvement with various choices on the weighted loss. Moreover, practical techniques for fine-tuning pretrained diffusion policies have also been proposed in DPPO (Ren et al., 2024). Furthermore, FPO (McAllister et al., 2025) and GenPO (Ding et al., 2025) develop different tricks to approximate the log likelihood of the diffusion policy and try

to optimize the diffusion policy with PPO loss (Schulman et al., 2017). However, existing diffusion-based RL methods mostly focus on the diffusion policy and overlook how to effectively utilize the diffusion model as a powerful critic. In that case, our DBC is proposed to tackle the absence of efficient diffusion-based critics.

Distributional Critic Learning. Distributional reinforcement learning aims to learn the full probability distribution of value functions rather than merely estimating their expectations (Bellemare et al., 2017; 2023). Early methods primarily rely on discretization or parametric assumptions. C51 discretizes the Q-value support into a fixed set of atoms and learns a categorical distribution (Bellemare et al., 2017). QR-DQN learns discrete quantiles via quantile regression (Dabney et al., 2018b), and IQN further introduces implicit quantile networks that map arbitrary probability levels to corresponding Q-values, enabling more flexible distributional representations (Dabney et al., 2018a). For continuous control, DSAC imposes Gaussian assumptions on value distributions within the SAC framework (Duan et al., 2022; 2025), while TQC improves stability through ensembles of quantile critics (Kuznetsov et al., 2020). Despite their effectiveness, these methods remain constrained by discrete supports or fixed parametric forms, limiting their capacity to capture complex value distribution structures. Very recently, diffusion and flow matching models have emerged as more expressive alternatives for value distribution learning. Diffusion models learn multimodal value distributions through iterative denoising (Hu et al., 2025; Zhong et al., 2025b), consistency models enable efficient uncertainty estimation via single-step sampling (Zhang et al., 2024), and flow matching approaches either compute Q-functions iteratively through learned velocity fields (Agrawalla et al., 2025) or directly model return distributions generatively (Zhong et al., 2025a; Chen et al., 2025; Dong et al., 2025).

Nevertheless, existing generative methods either rely on iterative sampling for scalar value estimation or introduce implicit distributional assumptions when generating return samples. In contrast, our method leverages diffusion bridges to learn the inverse cumulative distribution function, enabling explicit value distribution modeling within a unified quantile framework.

3. Preliminaries

3.1. Distributional Reinforcement Learning

Consider a Markov Decision Process (MDP) defined by the quintuple $(\mathcal{S}, \mathcal{A}, \mathcal{P}, \mathcal{R}, \gamma)$. Here, \mathcal{S} and \mathcal{A} denote the state and action spaces, respectively, with state $s \in \mathcal{S}$ and action $a \in \mathcal{A}$ both represented as vectors. The state transition probability density is given by $\mathcal{P} : \mathcal{S} \times \mathcal{A} \rightarrow \Delta(\mathcal{S})$, $\mathcal{R}(s, a)$ is a stochastic reward function, and $\gamma \in [0, 1)$ is the discount

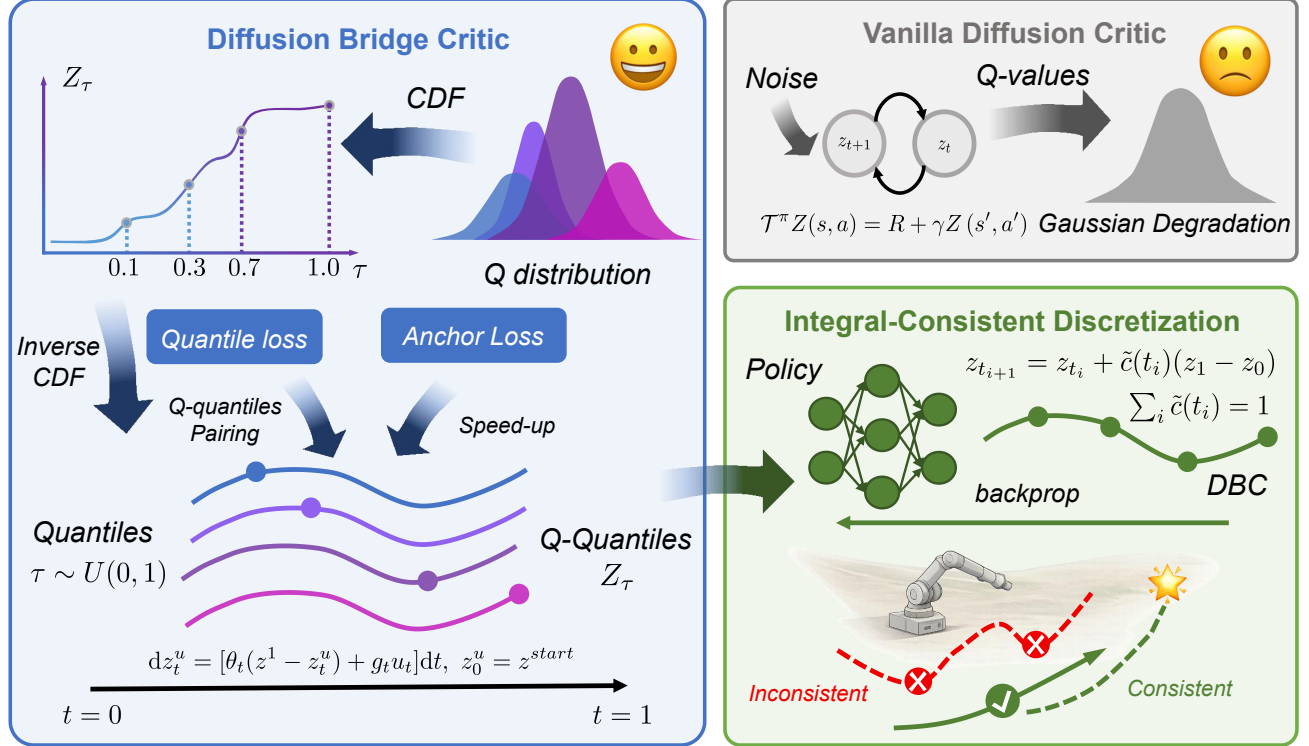


Figure 1. The training pipeline of Diffusion Bridge Critics. Compared with Vanilla Diffusion Critic, DBC explicitly models the inverse cumulative distribution function (CDF) of Q-values and resolves the Gaussian Degradation Problem. Besides, the design of the integral-consistent discretization technique is also developed for accurate value estimation and stable policy optimization.

factor. A policy $\pi : \mathcal{S} \rightarrow \mathcal{A}$ maps states to actions.

The random return $Z^\pi(s, a)$ is defined as the discounted sum of future rewards $r_k \in \mathcal{R}$:

$$Z^\pi(s, a) = \sum_{k=0}^{\infty} \gamma^k r_k, \quad s_0 = s, \quad a_0 = a, \quad (1)$$

$a_k \sim \pi(\cdot | s_k), \quad s_{k+1} \sim \mathcal{P}(\cdot | s_k, a_k).$

In contrast to traditional reinforcement learning, which estimates the expected return $Q^\pi(s, a) = \mathbb{E}[Z^\pi]$, distributional reinforcement learning aims to model the full distribution of the one-dimensional random variable Z^π . The distributional Bellman operator \mathcal{T}^π is defined as:

$$\mathcal{T}^\pi Z(s, a) \stackrel{D}{=} \mathcal{R}(s, a) + \gamma Z(s', \pi(s')), \quad s' \sim \mathcal{P}(\cdot | s, a), \quad (2)$$

where $\stackrel{D}{=}$ denotes equality in distribution. Under the p -Wasserstein distance, \mathcal{T}^π is a γ -contraction operator [citation], which guarantees the existence and uniqueness of its distributional fixed point.

We characterize the distribution via its quantile function $F_{Z(s, a)}^{-1}(\tau)$, where $\tau \in [0, 1]$ is the quantile level.

$$\begin{aligned} \mathcal{L}_{QR}(\theta) &= \mathbb{E}_{(s, a) \sim \mathcal{D}, \tau \sim U([0, 1])} [\rho_\tau^\kappa(y - f_\theta(s, a, \tau))] , \\ \rho_\tau^\kappa(u) &= |\tau - \mathbb{I}(u < 0)| \cdot \mathcal{L}_\kappa^{\text{Huber}}(u) \end{aligned} \quad (3)$$

where y is the target sample and $\mathcal{L}_\kappa^{\text{Huber}}$ is the huber loss with parameter κ .

We provide a detailed derivation of the empirical quantile and proofs of the related results in [Appendix C](#).

3.2. Diffusion Bridge

Diffusion bridge models have achieved significant success across a range of applications, including image translation (Liu et al., 2023; Li et al., 2023; Zhou et al., 2023; Albergo et al., 2023), image restoration (Luo et al., 2023; Yue et al., 2024; Zhu et al., 2025; Wang et al., 2025), and video generation (Wang et al., 2024a), which overcome the limitation of Gaussian prior in standard diffusion models. UniDB (Zhu et al., 2025) is a unified framework demonstrating that h -transform-based models (Zhou et al., 2023; Yue et al., 2024) can be unified through the lens of Stochastic Optimal Control (SOC) theory. To model the transition starting from a sample z^{start} in prior distribution to z^{end} data distribution, UniDB (Zhu et al., 2025) constructed the following Linear Quadratic Optimal Control problem (Kappen, 2008; Chen et al., 2023) as

$$\begin{aligned} \min_{u_t} \int_0^1 \frac{1}{2} \|u_t\|_2^2 dt + \frac{\gamma}{2} \|z_1^u - z^{end}\|_2^2 \\ \text{s.t. } dz_t^u = [\theta_t(z^{end} - z_t^u) + g_t u_t]dt, \quad z_0^u = z^{start}, \end{aligned} \quad (4)$$

where x_t^u is the controlled diffusion process, u_t is the controller, $\int_0^1 \frac{1}{2} \|u_t\|_2^2 dt$ is the transient cost, $\frac{\gamma}{2} \|x_1^u - z^{\text{end}}\|_2^2$ is the terminal cost with its penalty coefficient γ , θ_t and g_t are two scalar-valued functions with a relationship $g_t^2 = 2\lambda^2\theta_t$ where the steady variance level λ^2 is a given constant. Here we directly consider the deterministic optimal control problem (4) with fixed endpoints ($\gamma \rightarrow \infty$ to make the controlled dynamics precisely converge to z^{end}) (Chen et al., 2023) in UniDB because in the context of distributional reinforcement learning, the relationship between the boundary samples z^{start} and z^{end} is deterministic. According to Pontryagin Maximum Principle (Kappen, 2008), UniDB provided the solution to the SOC problem Eq. (4) and the corresponding transition z_t between z^{start} and z^{end} as

$$z_t^u = \xi(t)z^{\text{start}} + (1 - \xi(t))z^{\text{end}}, \quad \xi(t) = e^{-\bar{\theta}_{0:t}} \frac{\bar{\sigma}_{t:1}^2}{\bar{\sigma}_{0:1}^2}, \quad (5)$$

where $\bar{\theta}_{s:t} = \int_s^t \theta_z dz$ and $\bar{\sigma}_{s:t}^2 = \lambda^2(1 - e^{-2\bar{\theta}_{s:t}})$. For more details, please refer to UniDB (Zhu et al., 2025).

4. Diffusion Bridge Critic

In this section, we first reveal the Gaussian degradation problem in vanilla diffusion critic. To address this issue and sufficiently utilize the expressiveness of the diffusion bridge model, we propose the **Diffusion Bridge Critic** (DBC). With the quantile loss, it models the Q-value distribution as a "bridge" between quantiles τ and the corresponding Q-quantiles Z_τ . Besides, we also design an anchor loss to reduce the training variance and speed up the convergence. Moreover, we further investigate the impact of DBC on policy improvement. Since the implementation of DBC is actually the discretization of diffusion bridges, we propose an integral-consistent discretization technique to calibrate the parameters of DBC, thereby providing accurate value estimates for policy improvement. The full pipeline of DBC is shown in Figure 1.

4.1. Limitation of Vanilla Diffusion Critics

As we mentioned before, diffusion critics tend to collapse to a trivial Gaussian distribution due to their distribution learning paradigm. Intuitively, the approximation errors in the TD target can be continuously accumulated by the Bellman operator under the diffusion-critic training paradigm, causing the learned distribution to gradually converge toward a Gaussian distribution, as suggested by the central limit theorem.

Theorem 4.1 (Gaussian Degradation of Diffusion Critics). *Diffusion Critics f_θ finally degrades into a Gaussian distri-*

Algorithm 1 Training for DBC

Input: replay buffer \mathcal{D} , online parameters θ , target parameters ϕ , heads H , discount γ , atoms K_{target}

- 1: **for** $i = 1$ **to** N **do**
- 2: Sample $(s, a, r, s', \text{done}) \sim \mathcal{D}$, and sample $a' \sim \pi(\cdot | s')$
- 3: Generate target value $\{z_i\}_{i=1}^{K_{\text{tgt}}}$ by Eq. 20
- 4: Build target sample $\mathcal{Y} = \{y_i\}_{i=1}^{K_{\text{target}}}$ by Eq. (7).
- 5: Sample $\tau_i \sim U([0, 1])$ and set $z^{\text{start}}(\tau_i) \leftarrow \tau_i$
- 6: Calculate $\{y_i^{\text{emp}}\}_{i=1}^K$ according to Eq. (10)
- 7: **for** $h = 1$ **to** H **do**
- 8: Calculate $\mathcal{L}^{(h)}$ according to Eq. (12)
- 9: **end for**
- 10: Update θ using $\frac{1}{H} \nabla_\theta \sum_{h=1}^H \mathcal{L}^{(h)}$
- 11: Soft update for target network.
- 12: **end for**

bution $\mathcal{N}(Q(s, a), \sigma^2)$ under the Bellman backup operator:

$$\mathcal{T}^\pi Z(s, a) = R(s, a) + \gamma Z(s', a'), \quad Z \sim f_\theta(s, a).$$

The proof can be referred to in [Appendix A](#).

Besides, we also provide a toy example to illustrate that directly applying diffusion and flow matching methods to distributional RL leads to a tendency toward Gaussian distributions as bootstrapping training iterations progress in Figure 2. In contrast, DBC avoids this issue by explicitly modeling the relationship between z^{start} and z^{end} since it fits the mapping of the inverse CDF of the Q-value distribution instead of directly modeling the Q-value distribution. We provide detailed analyses in [Appendix A](#).

4.2. Training Process of DBC

To resolve the Gaussian degradation problem, we propose diffusion bridge critics, which adopts a quantile-function parameterization for the distributional critic. Given a state-action pair (s, a) , a quantile level $\tau \in (0, 1)$, and a bridge time $t \in [0, 1]$, the online network directly predicts the data endpoint

$$\hat{z}_{\tau, t} = f_\theta(z_t, t, \tau, s, a), \quad (6)$$

where z_t is an intermediate variable along the diffusion bridge trajectory Eq. (5). Since our training objectives are defined at the data endpoint z^{end} (i.e., return particles), we employ a *data-prediction* parameterization so that the supervision acts directly on z^{end} , avoiding time-scale reweighting and error propagation induced by additional parameter transformations.

For each critic update, we use a target network to generate a set of target return particles by Eq. (4). Concretely, the target critic samples $\{z_j^{\text{target}}\}_{j=1}^{K_{\text{tgt}}}$ at the next state-action pair (s', a') through the bridge Eq. (4), and we apply a

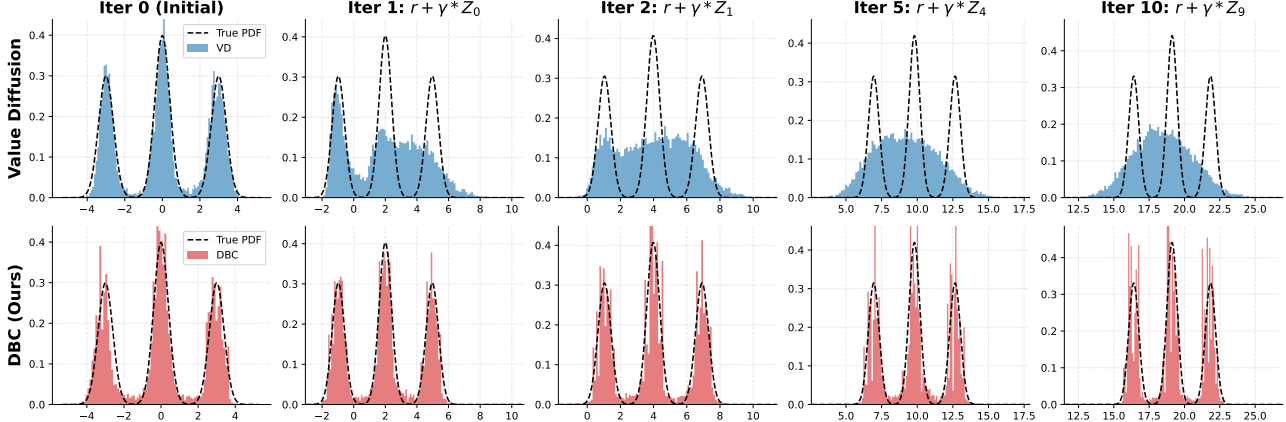


Figure 2. Top row: Value diffusion fits the iterative target $r + \gamma \cdot Z_{k-1}^{\text{FM}}$. Bottom row: DBC fits the iterative target $r + \gamma \cdot Z_{k-1}^{\text{DBC}}$. DBC introduces quantile conditioning τ , which consequently preserves multimodality of the distribution under iterative Bellman drift $Z_k \leftarrow r + \gamma Z_{k-1}$. We take 100 inner training steps to fit Z_k for each method in iteration and 10000 steps to fit the initial distribution in Iter 0.

Bellman transform to obtain

$$\mathcal{Y} = \{y_j\}_{j=1}^{K_{\text{tgt}}}, \quad y_j := r + \gamma z_j^{\text{target}}. \quad (7)$$

Given \mathcal{Y} , we jointly optimize two losses: a standard quantile loss and an *anchor loss*.

Following prior quantile-based distributional RL methods, we regress each predicted quantile to the target particle distribution using the huberized quantile loss:

$$\mathcal{L}_t^{\text{quantile}} = \sum_{j=1}^{K_{\text{tgt}}} \sum_{i=1}^{K_{\text{onl}}} \rho_{\tau_i}^{\kappa} \left(y_j - f_{\theta}(z_t, t, \tau_i, s, a) \right), \quad (8)$$

where $\{\tau_i\}_{i=1}^{K_{\text{onl}}} \subset (0, 1)$ are quantile levels, K_{onl} represents the number of samples generated by nline network. This objective exploits all particles to capture the distributional shape. However, the supervision for each τ_i is *implicit*, the network must infer the quantile location through comparisons to all y_j , and the resulting gradient estimator can have high variance, which may slow down the early formation of a well-structured quantile function and destabilize training.

Anchor loss. To provide a more direct and lower-variance learning signal, we introduce an estimator for quantile. Let the order statistics of \mathcal{Y} be

$$y_{(1)} \leq y_{(2)} \leq \dots \leq y_{(K_{\text{tgt}})}. \quad (9)$$

We define the sample τ -quantile by

$$y^{\text{sample}}(\tau) := y_{(\lceil K_{\text{tgt}} \tau \rceil)}. \quad (10)$$

Importantly, $y^{\text{sample}}(\tau)$ is not a heuristic label: it can be characterized as a **minimizer of Eq. (8)** with $\kappa = 0$, i.e., it is the explicit solution obtained by solving Eq. (8) with fixed

samples \mathcal{Y} . We provide a formal proof of this relationship and further properties of empirical quantiles in Appendix C. Thus, we can build z_t by $y^{\text{sample}}(\tau)$ and τ . For $t = 0$, we directly set $z_t = \tau$. Using these anchors, we impose an explicit pointwise regression term with a robust Huber penalty:

$$\mathcal{L}_t^{\text{Anchor}} = \sum_{i=1}^{K_{\text{onl}}} \mathcal{L}_{\kappa}^{\text{Huber}} \left(f_{\theta}(z_t, t, \tau_i, s, a) - y^{\text{sample}}(\tau_i) \right). \quad (11)$$

This anchor loss provides direct supervision for each τ_i , reducing optimization ambiguity and gradient variance, and accelerating the early shaping of the quantile function. While it does not impose a hard monotonicity constraint, the anchored targets $\tau_i \mapsto y^{\text{sample}}(\tau_i)$ are naturally ordered, which encourages more consistent quantile structure and mitigates quantile crossing in practice.

We train the critic with the weighted combination

$$\mathcal{L}_t = \mathcal{L}_t^{\text{quantile}} + w \cdot \mathcal{L}_t^{\text{Anchor}}, \quad (12)$$

where $w \geq 0$ controls the anchoring strength. However, relying solely on the anchor loss is not recommended, as the anchor **provides a biased target in expectation**, with the bias magnitude on the order of $o\left(\frac{1}{\sqrt{K_{\text{tgt}}}}\right)$. We provide a detailed analysis and discussion in Theorem C.4. For conditioning, we encode both the quantile level τ and the bridge time t using cosine embeddings and inject them into the critic. To mitigate value overestimation during critic updates, we adopt a DropTop aggregation strategy, which discards the largest quantile estimates and aggregates the remaining ones to obtain a conservative value estimate, following prior work on quantile-based critics (Kuznetsov et al., 2020).

For gradient-based methods such as SAC and TD3, whose policy updates rely on gradients of the return estimate, the backpropagation is performed through the entire sampling procedure.

Although the diffusion bridge defines a deterministic trajectory from z^{start} to z^{end} , naive Euler discretization and iterative sampling may introduce **numerical errors and endpoint bias**. We discuss this issue and the corresponding remedies in the next section.

4.3. Integral-consistent Discretization of DBC

In the previous section, we described how DBC is trained. However, Eq. (4) cannot be directly used to generate rewards for the policy. In practice, this equation must be discretized in order to be iteratively evaluated. Unfortunately, commonly used discretization schemes introduce *endpoint bias* when applied to diffusion bridges. This bias causes the policy network to be optimized with respect to wrong reward signals, which can lead to training instability or even collapse. To address this issue, we propose an *integral-consistent discretization* scheme in this section. A brief description of the proposed algorithm is provided in Algorithm 2.

To make the source of endpoint bias explicit, we rewrite the UniDB solution in Eq. (5) and substitute it into the controlled dynamics in Eq. (4). This yields the following deterministic ODE along the bridge:

$$\frac{dz_t}{dt} = c(t) (z^{\text{end}} - z^{\text{start}}), \quad c(t) = \left(\theta_t + g_t^2 \frac{e^{-2\bar{\theta}_{t:1}}}{\bar{\sigma}_{t:1}^2} \right) \xi(t), \quad (13)$$

where $z_t \in \mathbb{R}$ denotes the scalar return value at time t , and $(z^{\text{start}}, z^{\text{end}})$ are the prescribed boundary endpoints. For the continuous-time trajectory to satisfy $z_0 = z^{\text{start}}$ and $z_1 = z^{\text{end}}$, the velocity coefficient must satisfy the global constraint

$$\int_0^1 c(t) dt = 1. \quad (14)$$

Algorithm 2 Integral-consistent ODE Sampling for DBC

Input: online critic f_θ , state-action (s, a) , quantiles $\{\tau_i\}_{i=1}^K$ **Hyperparameters:** time grid $\{t_m\}_{m=0}^M$, interpolation $\xi(\cdot)$

```

1: for  $i = 1$  to  $K$  (In Parallel) do
2:    $z \leftarrow z^{\text{start}} \leftarrow \tau_i$ 
3:   for  $m = 0$  to  $M - 1$  do
4:      $\hat{z}_{\tau, t_m} \leftarrow f_\theta(z, t_m, \tau_i, s, a)$ 
5:      $z \leftarrow z + \tilde{c}(t_m)(\hat{z}_{\tau, t_m} - z^{\text{start}})$ 
6:   end for
7:    $z_{(i)}^1 \leftarrow z$ 
8: end for

```

Let $0 = t_0 < t_1 < \dots < t_M = 1$ be an arbitrary time partition. A conventional Euler discretization applies the update

$$z_{t_{i+1}} = z_{t_i} + c(t_i) \Delta t_i (z^{\text{end}} - z^{\text{start}}), \quad \Delta t_i = t_{i+1} - t_i. \quad (15)$$

After M steps, the accumulated displacement becomes

$$z_{t_M} - z_{t_0} = \left(\sum_{i=0}^{M-1} c(t_i) \Delta t_i \right) (z^{\text{end}} - z^{\text{start}}). \quad (16)$$

For finite M , the discrete sum $\sum_i c(t_i) \Delta t_i$ generally deviates from the continuous integral $\int_0^1 c(t) dt = 1$, resulting in $z_{t_M} \neq z^{\text{end}}$. We refer to this discrepancy as endpoint bias. Importantly, this discrepancy is not stochastic numerical noise but a systematic violation of the global boundary constraint. We provide a detailed analysis and empirical illustration of this endpoint bias in Appendix B.

We now show that endpoint bias can be eliminated entirely by enforcing integral consistency at the discretization level.

Theorem 4.2 (Endpoint Consistency via Integral-Consistent Discretization). *Let $z_t \in \mathbb{R}$ follow the ODE*

$$\frac{dz_t}{dt} = c(t) (z^{\text{end}} - z^{\text{start}}), \quad (17)$$

where $z^{\text{start}}, z^{\text{end}} \in \mathbb{R}$ are fixed endpoints and $c : [0, 1] \rightarrow \mathbb{R}$ is integrable with $\int_0^1 c(t) dt = 1$. For any partition $0 = t_0 < t_1 < \dots < t_M = 1$, define the discrete update by exact interval integration:

$$z_{t_{i+1}} = z_{t_i} + \left(\int_{t_i}^{t_{i+1}} c(t) dt \right) (z^{\text{end}} - z^{\text{start}}). \quad (18)$$

Then the resulting discrete trajectory satisfies $z_{t_M} = z^{\text{end}}$ whenever $z_{t_0} = z^{\text{start}}$, independent of M and the choice of partition.

We note the following identity between the interpolation coefficient $\xi(t)$ and the velocity coefficient $c(t)$:

$$c(t) = -\frac{d\xi(t)}{dt}, \quad (19)$$

with boundary conditions $\xi(0) = 1$ and $\xi(1) = 0$. A formal proof is provided in Appendix B.

As a direct consequence, it leads to the following corollary.

Corollary 4.3 (Integral-consistent discretization for DBC). *For any partition $0 = t_0 < t_1 < \dots < t_M = 1$, set $\tilde{c}(t_i) := \xi(t_i) - \xi(t_{i+1})$, the update rule*

$$z_{t_{i+1}} = z_{t_i} + \tilde{c}(t_i)(z^{\text{end}} - z^{\text{start}}) \quad (20)$$

is integral-consistent and guarantees strict endpoint consistency $z_{t_M} = z^{\text{end}}$ for any number of steps M .

Table 1. Mean evaluation performance of different algorithms in the 5 MuJoCo benchmarks. All experiments are conducted with three random seeds. The returns reported in the tables are the averages of the best-performing results across these seeds.

Run	Ant-v5	HalfCheetah-v5	Hopper-v5	Humanoid-v5	Walker2d-v5
SAC	6121.8 ± 412.7	12776.4 ± 285.2	3630.5 ± 50.0	5207.1 ± 94.1	4854.4 ± 372.8
IQN	3487.4 ± 798.5	10930.2 ± 152.7	3301.8 ± 360.1	4729.2 ± 580.5	4766.5 ± 255.7
TQC	6342.6 ± 294.7	13996.2 ± 191.7	3704.6 ± 94.5	5269.0 ± 113.8	5802.6 ± 234.2
VD	3850.4 ± 987.1	4284.8 ± 478.2	1052.7 ± 20.4	4886.9 ± 228.8	2533.9 ± 302.4
VF	2650.3 ± 163.8	8199.5 ± 1533.3	3310.4 ± 24.6	4950.3 ± 60.3	2626.4 ± 1387.4
DSAC	2013.2 ± 679.9	12974.0 ± 191.7	3522.9 ± 23.5	3442.6 ± 216.8	3297.4 ± 1248.3
DBC(*)	6501.4 ± 84.3	13787.8 ± 346.5	3732.5 ± 83.2	5906.7 ± 198.6	6138.2 ± 38.1

This discretization exactly preserves the global geometry of the continuous bridge while requiring only evaluations of $\xi(t)$, without numerical quadrature or step-size tuning. As a result, DBC maintains stable generative semantics and strict endpoint consistency even with as few as $M = 5$ inference steps, which is critical for low-latency online reinforcement learning. We provide a concise for our sampling process in Algorithm 2.

Policy training. After the critic is fully trained, we use the online network to generate K_{onl} return samples via Algorithm 2. These samples are averaged to obtain an expected return estimate q_{onl} , which is then provided to the actor for policy optimization. We provide a brief overview of our method in Algorithm 1.

5. Experiments

In this section, we systematically evaluate the performance of DBC on multiple MuJoCo continuous-control benchmarks. We first compare DBC against several representative critic baselines to quantify its overall performance gains. We then assess DBC as a plug-and-play critic module by integrating it into different actor algorithms, thereby validating its generality across actor backbones. Finally, we conduct two ablation studies to analyze how key hyperparameters affect performance and training stability, including the flow steps M and the anchor loss weight w .

5.1. Comparative Evaluation

We benchmark DBC against several critic baselines, including SAC (Haarnoja et al., 2018), DSAC (Duan et al., 2022), IQN (Dabney et al., 2018a), TQC (Kuznetsov et al., 2020), Value Diffusion (VD) (Hu et al., 2025), and Value Flows (VF) (Dong et al., 2025), all implemented within our codebase. Brief descriptions of these baselines are provided in Appendix E. Table 1 presents the main results. For a controlled comparison, all baseline methods use a unified SAC actor backbone; for DBC, we additionally report the TD3-based variant on HalfCheetah-v5. Detailed experimental settings are provided in Appendix F, and the complete

breakdowns per-actor are reported in Appendix G.

In Table 1, all baselines are trained for 10^6 environment steps and evaluated over three random seeds. As shown, DBC achieves the best overall performance. DSAC exhibits a similar behavior, as it explicitly parameterizes the return distribution with a single Gaussian, limiting its capacity to represent rich, potentially multimodal return distributions. Learning curves of these baselines are demonstrated in Figure 3.

5.2. DBC as a plug-and-play module.

To validate the effectiveness of DBC as a plug-and-play critic module, we integrate it into three representative actor algorithms, SAC, TD3, and QVPO, and evaluate the resulting methods on two challenging continuous-control benchmarks, Humanoid-v5 and Walker2d-v5. As shown in Table 2, replacing CDQ with DBC consistently improves performance across all actor backbones. In particular, on Humanoid-v5, DBC yields a maximum improvement of 13% when paired with the SAC actor, while on Walker2d-v5, it achieves up to a 24% performance gain when integrated with TD3.

Table 2. DBC as a Plug-and-Play Critic Module Across Actors on Humanoid-v5 and Walker2d-v5 benchmarks.

Actor	Critic	Humanoid-v5	Walker2d-v5
QVPO	CDQ	5068.3 ± 28.5	4986.3 ± 279.6
	DBC(*)	5426.3 ± 9.0	5448.1 ± 193.8
SAC	CDQ	5207.1 ± 94.1	4854.4 ± 372.8
	DBC(*)	5906.7 ± 198.6	6138.2 ± 38.1
TD3	CDQ	5067.8 ± 33.7	5093.7 ± 439.8
	DBC(*)	5343.2 ± 199.3	6335.5 ± 269.4

5.3. Ablation Study

5.3.1. TIME STEPS

We ablate the number of time steps M to validate that our multi-step critic offers substantial gains beyond a naive integration of Diffusion Models and RL. As shown in Table 3, $M = 5$ outperforms $M = 1$ in all tasks, confirming that multi-step processing significantly enhances the ability to

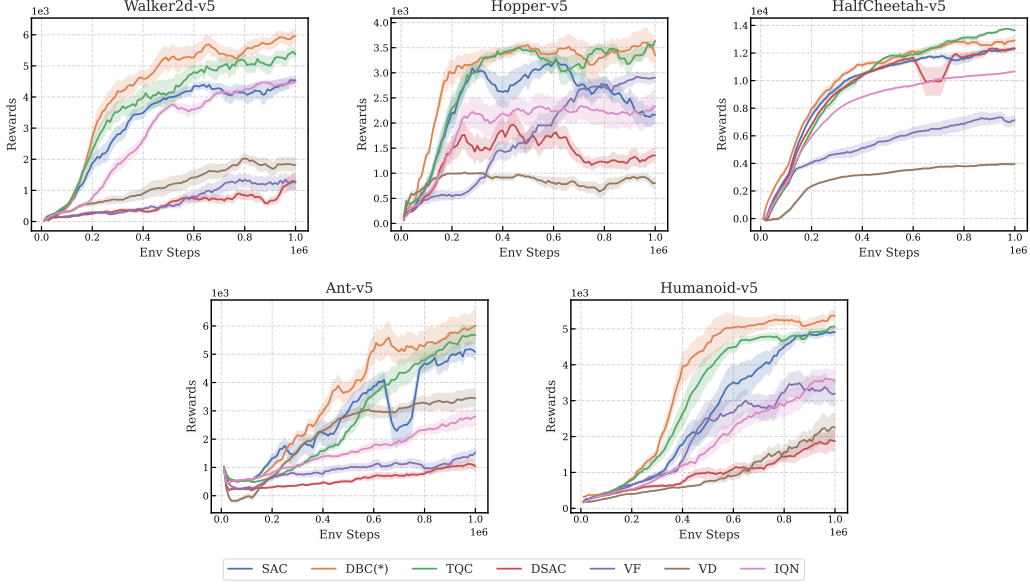


Figure 3. Learning curves of different algorithms on five MuJoCo benchmarks. The x-axis denotes training epochs, and the y-axis denotes episodic return. Curves are smoothed for improved visualization.

fit. However, increasing M to 10 introduces instability due to extended backpropagation chains. Therefore, we recommend $M = 5$ as the optimal trade-off between performance, cost, and stability.

Table 3. Ablation of Flow Steps M .

Run	Ant-v5	Humanoid-v5	Walker2d-v5
M=1	5150.4 \pm 2226.3	5524.7 \pm 132.7	5809.8 \pm 308.6
M=5	6501.4 \pm 84.3	5906.7 \pm 198.6	6138.2 \pm 38.1
M=10	5946.6 \pm 379.7	4848.7 \pm 88.1	6014.3 \pm 561.6

5.3.2. WEIGHT FOR ANCHOR LOSS

Finally, we analyze the effect of the anchor loss introduced in Section 4.2. Recall that our critic objective in Eq. (12) combines the quantile loss in Eq. (8) with an anchor term Eq. (11) weighted by w . Table 4 shows that adding a small anchor weight consistently improves performance: $w = 0.01$ achieves the best results on Ant-v5, Humanoid-v5, and Walker2d-v5, outperforming the $w = 0$ baseline that uses Eq. (8) alone. In contrast, larger weights (e.g., $w \geq 0.02$) can degrade performance, indicating that over-emphasizing the anchor term may distort the training objective. This is because the objective is biased as we have discussed before. Moreover, removing Eq. (8) leads to a substantial performance drop across all tasks, confirming that the quantile loss is essential for learning the distributional structure while the anchor loss is most effective as a auxiliary signal. Based on these results, $w = 0.01$ is

recommended.

Table 4. Ablation of Loss Weight w .

Run	Ant-v5	Humanoid-v5	Walker2d-v5
$w = 0.0$	4828.3 \pm 1439.0	5807.3 \pm 175.8	5562.9 \pm 423.2
$w = 0.01$	6501.4 \pm 84.3	5906.7 \pm 198.6	6138.2 \pm 38.1
$w = 0.02$	3947.3 \pm 2151.8	5743.4 \pm 301.1	6097.8 \pm 375.1
$w = 0.1$	5716.2 \pm 741.3	5589.0 \pm 50.3	5974.6 \pm 603.2
No Eq. (8)	2517.1 \pm 2464.7	3751.2 \pm 321.1	3859.3 \pm 1828.7

6. Conclusion

In this work, we revisit diffusion-based reinforcement learning from the perspective of value estimation and propose Diffusion Bridge Critics (DBC), a novel distributional RL method that leverages diffusion bridge models to accurately capture the Q-value distribution. By learning the inverse cumulative distribution function of Q-value distribution, DBC avoids the discrete quantile approximation and the Gaussian degradation that arises in vanilla diffusion critics under Bellman backups. Moreover, we derive an integral-consistent discretization to correct the bias induced by finite diffusion steps, leading to more accurate and stable value estimation. As a plug-and-play component, DBC can be seamlessly integrated into existing RL algorithms, and empirical results on MuJoCo benchmarks demonstrate consistent performance gains over prior distributional critics. These findings highlight the importance of expressive and reliable diffusion-based critics, and suggest that improving value estimation is a key direction for advancing diffusion-based RL.

Acknowledgement

This work was supported by National Natural Science Foundation of China (62303319, 62406195), Shanghai Local College Capacity Building Program (23010503100), ShanghaiTech AI4S Initiative SHTAI4S202404, HPC Platform of ShanghaiTech University, and MoE Key Laboratory of Intelligent Perception and Human-Machine Collaboration (ShanghaiTech University), Shanghai Engineering Research Center of Intelligent Vision and Imaging. This work was also supported in part by computational resources provided by Fcloud CO., LTD.

Impact Statement

This work focuses on improving value estimation in reinforcement learning by introducing diffusion bridge models as critics. By enabling more accurate distributional critic, DBC has the potential to enhance the reliability and efficiency of reinforcement learning systems, particularly in robotics and continuous control applications.

References

Agrawalla, B., Nauman, M., Agrawal, K., and Kumar, A. floq: Training critics via flow-matching for scaling compute in value-based rl. *arXiv preprint arXiv:2509.06863*, 2025.

Ajay, A., Du, Y., Gupta, A., Tenenbaum, J., Jaakkola, T., and Agrawal, P. Is conditional generative modeling all you need for decision-making? *arXiv preprint arXiv:2211.15657*, 2022.

Albergo, M. S., Boffi, N. M., and Vanden-Eijnden, E. Stochastic interpolants: A unifying framework for flows and diffusions. *arXiv preprint arXiv:2303.08797*, 2023.

Bellemare, M. G., Dabney, W., and Munos, R. A distributional perspective on reinforcement learning. In *International conference on machine learning*, pp. 449–458. PMLR, 2017.

Bellemare, M. G., Dabney, W., and Rowland, M. *Distributional reinforcement learning*. MIT Press, 2023.

Celik, O., Li, Z., Blessing, D., Li, G., Palanicek, D., Peters, J., Chalvatzaki, G., and Neumann, G. Dime: Diffusion-based maximum entropy reinforcement learning. *arXiv preprint arXiv:2502.02316*, 2025.

Chen, D., Liu, Y., Zhou, Z., Qu, C., and Qi, Y. Unleashing flow policies with distributional critics. *arXiv preprint arXiv:2509.23087*, 2025.

Chen, T., Gu, J., Dinh, L., Theodorou, E. A., Susskind, J., and Zhai, S. Generative Modeling with Phase Stochastic Bridges. *arXiv preprint arXiv:2310.07805*, 2023.

Chi, C., Feng, S., Du, Y., Xu, Z., Cousineau, E., Burchfiel, B., and Song, S. Diffusion policy: Visuomotor policy learning via action diffusion. *arXiv preprint arXiv:2303.04137*, 2023.

Dabney, W., Ostrovski, G., Silver, D., and Munos, R. Implicit quantile networks for distributional reinforcement learning. In *International conference on machine learning*, pp. 1096–1105. PMLR, 2018a.

Dabney, W., Rowland, M., Bellemare, M., and Munos, R. Distributional reinforcement learning with quantile regression. In *Proceedings of the AAAI conference on artificial intelligence*, volume 32, 2018b.

Ding, S., Hu, K., Zhang, Z., Ren, K., Zhang, W., Yu, J., Wang, J., and Shi, Y. Diffusion-based reinforcement learning via q-weighted variational policy optimization. *arXiv preprint arXiv:2405.16173*, 2024.

Ding, S., Hu, K., Zhong, S., Luo, H., Zhang, W., Wang, J., Wang, J., and Shi, Y. Genpo: Generative diffusion models meet on-policy reinforcement learning. *arXiv preprint arXiv:2505.18763*, 2025.

Dong, P., Zheng, C., Finn, C., Sadigh, D., and Eysenbach, B. Value flows. *arXiv preprint arXiv:2510.07650*, 2025.

Duan, J., Guan, Y., Li, S. E., Ren, Y., Sun, Q., and Cheng, B. Distributional soft actor-critic: Off-policy reinforcement learning for addressing value estimation errors. *IEEE Transactions on Neural Networks and Learning Systems*, 2022.

Duan, J., Wang, W., Xiao, L., Gao, J., Li, S. E., Liu, C., Zhang, Y.-Q., Cheng, B., and Li, K. Distributional soft actor-critic with three refinements. *IEEE Transactions on Pattern Analysis and Machine Intelligence*, 2025.

Fujimoto, S., Hoof, H., and Meger, D. Addressing function approximation error in actor-critic methods. In *International conference on machine learning*, pp. 1587–1596. PMLR, 2018.

Haarnoja, T., Zhou, A., Abbeel, P., and Levine, S. Soft actor-critic: Off-policy maximum entropy deep reinforcement learning with a stochastic actor. In *International conference on machine learning*, pp. 1861–1870. PMLR, 2018.

Hu, X., Wang, F., Zhang, T., and Cui, Z. Value diffusion reinforcement learning. In *The Thirty-ninth Annual Conference on Neural Information Processing Systems*, 2025. URL <https://openreview.net/forum?id=thJ6aFoKrh>.

Janner, M., Du, Y., Tenenbaum, J. B., and Levine, S. Planning with diffusion for flexible behavior synthesis. *arXiv preprint arXiv:2205.09991*, 2022.

Kappen, H. Stochastic optimal control theory. *ICML, Helsinki, Radbound University, Nijmegen, Netherlands*, 2008.

Kuznetsov, A., Shvechikov, P., Grishin, A., and Vetrov, D. Controlling overestimation bias with truncated mixture of continuous distributional quantile critics. In *International conference on machine learning*, pp. 5556–5566. PMLR, 2020.

Lehmann, E. L. and Casella, G. *Theory of point estimation*. Springer, 1998.

Li, B., Xue, K., Liu, B., and Lai, Y.-K. Bbdm: Image-to-image translation with brownian bridge diffusion models. In *Proceedings of the IEEE/CVF conference on computer vision and pattern Recognition*, pp. 1952–1961, 2023.

Liu, G.-H., Vahdat, A., Huang, D.-A., Theodorou, E. A., Nie, W., and Anandkumar, A. I2SB: Image-to-image schrödinger bridge. *arXiv preprint arXiv:2302.05872*, 2023.

Luo, Z., Gustafsson, F. K., Zhao, Z., Sjölund, J., and Schön, T. B. Image restoration with mean-reverting stochastic differential equations. *arXiv preprint arXiv:2301.11699*, 2023.

Ma, H., Chen, T., Wang, K., Li, N., and Dai, B. Efficient online reinforcement learning for diffusion policy. *arXiv preprint arXiv:2502.00361*, 2025a.

Ma, X., Chen, J., Xia, L., Yang, J., Zhao, Q., and Zhou, Z. Dsac: Distributional soft actor-critic for risk-sensitive reinforcement learning. *Journal of Artificial Intelligence Research*, 83, 2025b.

McAllister, D., Ge, S., Yi, B., Kim, C. M., Weber, E., Choi, H., Feng, H., and Kanazawa, A. Flow matching policy gradients. *arXiv preprint arXiv:2507.21053*, 2025.

Psenka, M., Escontrela, A., Abbeel, P., and Ma, Y. Learning a diffusion model policy from rewards via q-score matching. *arXiv preprint arXiv:2312.11752*, 2023.

Ren, A. Z., Lidard, J., Ankile, L. L., Simeonov, A., Agrawal, P., Majumdar, A., Burchfiel, B., Dai, H., and Simchowitz, M. Diffusion policy policy optimization. *arXiv preprint arXiv:2409.00588*, 2024.

Schulman, J., Wolski, F., Dhariwal, P., Radford, A., and Klimov, O. Proximal policy optimization algorithms. *arXiv preprint arXiv:1707.06347*, 2017.

Van der Vaart, A. W. *Asymptotic statistics*, volume 3. Cambridge university press, 2000.

Wang, H., Jin, T., Lin, W., Wang, S., Huang, H., Ji, S., and Zhao, Z. Irbridge: Solving image restoration bridge with pre-trained generative diffusion models. *arXiv preprint arXiv:2505.24406*, 2025.

Wang, Y., Chen, Z., Chen, X., Wei, Y., Zhu, J., and Chen, J. Framebridge: Improving image-to-video generation with bridge models. *arXiv preprint arXiv:2410.15371*, 2024a.

Wang, Y., Wang, L., Jiang, Y., Zou, W., Liu, T., Song, X., Wang, W., Xiao, L., Wu, J., Duan, J., et al. Diffusion actor-critic with entropy regulator. *Advances in Neural Information Processing Systems*, 37:54183–54204, 2024b.

Wang, Z., Hunt, J. J., and Zhou, M. Diffusion policies as an expressive policy class for offline reinforcement learning. In *The Eleventh International Conference on Learning Representations*, 2022.

Yang, L., Huang, Z., Lei, F., Zhong, Y., Yang, Y., Fang, C., Wen, S., Zhou, B., and Lin, Z. Policy representation via diffusion probability model for reinforcement learning. *arXiv preprint arXiv:2305.13122*, 2023.

Yue, C., Peng, Z., Ma, J., Du, S., Wei, P., and Zhang, D. Image Restoration Through Generalized Ornstein-Uhlenbeck Bridge. In *International Conference on Machine Learning*, 2024.

Zhang, J., Fang, L., Shi, K., Wang, W., and Jing, B. Q-distribution guided q-learning for offline reinforcement learning: Uncertainty penalized q-value via consistency model. *Advances in Neural Information Processing Systems*, 37:54421–54462, 2024.

Zhong, S., Ding, S., Diao, H., Wang, X., Teh, K. C., and Peng, B. Flowcritic: Bridging value estimation with flow matching in reinforcement learning. *arXiv preprint arXiv:2510.22686*, 2025a.

Zhong, S., Wang, G., Zhang, J., Wang, X., Teh, K. C., Diao, H., Zhang, P., He, J., Zeng, Z., Cheng, T. H., et al. Mad3pg: A framework for multi-agent deep denoising diffusion policy gradient optimization. *Information Fusion*, pp. 104026, 2025b.

Zhou, L., Lou, A., Khanna, S., and Ermon, S. Denoising Diffusion Bridge Models. *arXiv preprint arXiv:2309.16948*, 2023.

Zhu, K., Pan, M., Ma, Y., Fu, Y., Yu, J., Wang, J., and Shi, Y. UniDB: A Unified Diffusion Bridge Framework via Stochastic Optimal Control. In *Forty-second International Conference on Machine Learning*, 2025.

A. Proof

A.1. Proof of Theorem 4.1

Theorem A.1. Gaussian Degradation of Diffusion Critics. Vanilla Diffusion Critics f_θ finally degrades into a Gaussian distribution $\mathcal{N}(Q(s, a), \sigma^2)$ with the Bellman update:

$$\mathcal{T}^\pi Z(s, a) = R(s, a) + \gamma Z(s', a'), Z \sim f_\theta(s, a).$$

Proof. Due to the existence of approximation error ϵ_t in the t th Bellman expansion, the target distribution of diffusion is $\hat{Z}(s, a) = R(s, a) + \epsilon_0 + \gamma(\hat{Z}(s', a') + \epsilon_1)$. Hence, we can derive that

$$\hat{Z}(s, a) = Z(s, a) + \sum_{t=0}^{\infty} \gamma^t \epsilon_t.$$

Then, for convenience let $Z(s, a) = Q(s, a) + \gamma^{-1} \epsilon_{-1}$ rewrite the $\hat{Z}(s, a) = Z(s, a) + \sum_{t=-1}^{\infty} \gamma^t \epsilon_t = Q(s, a) + \sum_{t=-1}^{\infty} \gamma^t \epsilon_t$. Since the approximation error can be assumed to be independent of each other with zero mean, we can apply the Central Limit Theorem: when $\gamma \rightarrow 1$, we have

$$\hat{Z}(s, a) \rightarrow \mathcal{N}(Q(s, a), \sigma^2).$$

In that case, with Bellman backup iteration, the vanilla diffusion critics will finally fall into a Gaussian distribution. \square

Notably, the inherent problem here is that diffusion models are designed to model distributions rather than point-to-point mappings. In other words, the objective

$$\min_{\theta} \mathbb{E}_{\epsilon, t} \left[\left\| \epsilon - \epsilon_\theta \left(\sqrt{\bar{\alpha}_t} x + \sqrt{1 - \bar{\alpha}_t} \epsilon, t \right) \right\|^2 \right], \quad x = \mathbb{E}(Z),$$

is not equivalent to

$$\min_{\theta} \mathbb{E}_{Z, \epsilon, t} \left[\left\| \epsilon - \epsilon_\theta \left(\sqrt{\bar{\alpha}_t} Z + \sqrt{1 - \bar{\alpha}_t} \epsilon, t \right) \right\|^2 \right], \quad x = Z.$$

in the diffusion model. Therefore, the approximation error cannot be alleviated simply by collecting more samples (i.e., $\mathbb{E}(Z + \gamma \epsilon_t) = \mathbb{E}(Z)$).

In contrast, DBC establishes an explicit mapping from quantiles τ to the Q-value distribution Z_τ , rendering the two objectives equivalent. That corresponds to our quantile loss (8) and the anchor loss (11), which both drive the outputs of the diffusion bridge to converge to the corresponding Q-value quantiles Z_τ .

B. Integral-consistent Discretization

B.1. Proof for (19)

We formally establish the relationship between the time-dependent velocity coefficient $c(t)$ and the interpolation coefficient $\xi(t)$. Revisiting Eq. (5) from the main text:

$$\mathbf{u}_t^* = g_t \frac{e^{-2\bar{\theta}_{t:1}}}{\bar{\sigma}_{t:1}^2} (x_1 - x_t), \quad x_t = \xi(t)x_0 + (1 - \xi(t))x_1. \quad (5)$$

where $\xi(t)$ is a smooth scalar function satisfying the boundary conditions $\xi(1) = 0$ and $\xi(0) = 1$.

To derive the ordinary differential equation (ODE) governing this process, we differentiate Eq. (5) with respect to time t :

$$\begin{aligned} \frac{dx_t}{dt} &= \frac{d}{dt} [\xi(t)x_0 + x_1 - \xi(t)x_1] \\ &= \dot{\xi}(t)x_0 - \dot{\xi}(t)x_1 \\ &= -\dot{\xi}(t)(x_1 - x_0). \end{aligned} \quad (21)$$

B.2. Proof for Theorem 4.2

Proof. By explicitly expanding the discrete updates, we obtain

$$\begin{aligned}
 x_{t_M} &= x_{t_0} + \left(\int_{t_0}^{t_M} c(t) dt \right) (x_1 - x_0) \\
 &= x_{t_0} + (C(t_M) - C(t_0))(x_1 - x_0) \\
 &= x_0 + (C(1) - C(0))(x_1 - x_0) \\
 &= x_1,
 \end{aligned} \tag{22}$$

where we used the boundary conditions $x_{t_0} = x_0$, $t_0 = 0$, $t_M = 1$, and $C(1) - C(0) = 1$. \square

B.3. Schedules for θ

The behavior of the GOU bridge is governed by the drift coefficient $\theta(t)$. In our experiments, we evaluated three distinct schedule types. For all schedules, we set the hyperparameters $\theta_{\min} = 0.1$ and $\theta_{\max} = 5.0$.

Constant Schedule: The drift rate remains invariant throughout the process.

$$\theta(t) = 1.0 \tag{23}$$

Linear Schedule: The drift rate increases linearly, enforcing stronger mean-reversion near the target $t = 1$.

$$\theta(t) = \theta_{\min} + (\theta_{\max} - \theta_{\min}) \cdot t \tag{24}$$

Cosine Schedule: A smooth, non-linear schedule that transitions gently at the boundaries.

$$\theta(t) = \theta_{\min} + \frac{\theta_{\max} - \theta_{\min}}{2} (1 - \cos(\pi t)) \tag{25}$$

B.4. Quantitative Analysis of Endpoint Bias

Standard Euler discretization approximates the continuous integral $\int c(t)dt$ with a discrete sum $\sum c(t_i)\Delta t_i$. Due to the non-linearity of $c(t)$, particularly under dynamic drift schedules, this approximation introduces a systematic discrepancy that prevents the trajectory from reaching the intended boundary. We term this phenomenon **Endpoint Bias** and quantify it using the relative error $\mathcal{E} = |1 - \sum_{i=0}^{M-1} c(t_i)\Delta t_i| \times 100\%$.

Table 5 presents the errors calculated in various inference steps (M). The results reveal that standard Euler discretization incurs substantial bias, exceeding 21% in low-latency regimes ($M \leq 5$), which can lead to unstable generative semantics and inaccurate reward estimation in online reinforcement learning. In particular, while the Euler method requires a large number of steps ($M \geq 1000$) to suppress bias to negligible levels, our proposed **Integral-Consistent Discretization** mathematically eliminates this error, maintaining a consistent $\mathcal{E} = 0$ regardless of the number of steps or the complexity of the drift schedule.

Table 5. Relative endpoint error (%) of standard Euler discretization under different schedules and M .

Steps (M)	Euler Discretization Error (%)		
	Constant	Linear	Cosine
1	14.91	21.44	21.44
2	9.48	6.93	18.75
5	4.29	5.41	6.85
10	2.23	3.07	3.42
20	1.13	1.62	1.71
50	0.46	0.67	0.68
100	0.23	0.34	0.34
1000	0.02	0.03	0.03

C. Sample Quantile

This section presents a detailed analysis of the anchor proposed in the main text, focusing on its formal definition and asymptotic properties. Let X be a real-valued random variable with distribution function $F \in C^1$ and density $f = F'$, satisfying $\mathbb{E}[X^2] < \infty$. Let X_i be i.i.d. samples drawn from F , and denote the associated order statistics by

$$X_{(1)} \leq X_{(2)} \leq \dots \leq X_{(n)}.$$

The sample distribution function is defined as

$$\hat{F}_n(x) := \frac{1}{n} \sum_{i=1}^n \mathbb{I}(X_i \leq x),$$

where $\mathbb{I}(\cdot)$ denotes the indicator function. For a fixed quantile level $\tau \in (0, 1)$, the (generalized) empirical τ -quantile is defined via the generalized inverse

$$\hat{F}_n^{-1}(\tau) := \inf \{x \in \mathbb{R} : \hat{F}_n(x) \geq \tau\}.$$

It follows immediately that

$$\hat{F}_n^{-1}(\tau) = X_{(\lceil n\tau \rceil)}.$$

For notational convenience, we write $\hat{X}_\tau := \hat{F}_n^{-1}(\tau)$.

Sample quantiles as a empirical minimizer of the quantile loss. Define the quantile loss $\rho_\tau : \mathbb{R} \rightarrow \mathbb{R}$ by

$$\rho_\tau(u) = u(\tau - \mathbb{I}(u < 0)), \quad \forall u \in \mathbb{R}.$$

Consider the sample risk as a function of a scalar decision variable $\theta \in \mathbb{R}$:

$$L(\theta) := \sum_{i=1}^n \rho_\tau(X_i - \theta).$$

Then every minimizer of $L(\theta)$ is an sample τ -quantile.

Lemma C.1 (Sample quantile as a minimizer of the quantile loss). *Let $\tau \in (0, 1)$ and define*

$$n_<(\theta) := \sum_{i=1}^n \mathbb{I}(X_i < \theta), \quad n_{\leq}(\theta) := \sum_{i=1}^n \mathbb{I}(X_i \leq \theta).$$

Then the set of minimizers of $L(\theta)$ is

$$\arg \min_{\theta \in \mathbb{R}} L(\theta) = \{\theta \in \mathbb{R} : n_<(\theta) \leq n\tau \leq n_{\leq}(\theta)\}.$$

In particular, $\hat{X}_\tau = X_{(\lceil n\tau \rceil)}$ is always a minimizer. Moreover, if $X_{(\lceil n\tau \rceil)} < X_{(\lceil n\tau \rceil+1)}$ (i.e., there is no tie at the $\lceil n\tau \rceil$ -th order statistic), then the minimizer is unique and equals \hat{X}_τ .

Proof. For each i , define $\ell_i(\theta) = \rho_\tau(X_i - \theta)$. As a function of θ , ℓ_i is convex and piecewise linear. Its subgradient is

$$\partial \ell_i(\theta) = \begin{cases} \{-\tau\}, & X_i > \theta, \\ \{1 - \tau\}, & X_i < \theta, \\ [-\tau, 1 - \tau], & X_i = \theta, \end{cases}$$

where ∂ denotes the subdifferential (a set) in \mathbb{R} . By subdifferential calculus for sums of convex functions,

$$\partial L(\theta) = \sum_{i=1}^n \partial \ell_i(\theta).$$

Let $n_<(\theta)$ and $n_{\leq}(\theta)$ be defined as in the statement. Then the indices with $X_i < \theta$ contribute $1 - \tau$, those with $X_i > \theta$ contribute $-\tau$, and those with $X_i = \theta$ contribute an interval $[-\tau, 1 - \tau]$. Collecting terms yields

$$\partial L(\theta) = [n_<(\theta) - n\tau, n_{\leq}(\theta) - n\tau].$$

A point θ minimizes the convex function L if and only if $0 \in \partial L(\theta)$, which is equivalent to

$$n_<(\theta) \leq n\tau \leq n_{\leq}(\theta).$$

This proves the characterization of $\arg \min L(\theta)$. Since $\hat{X}_\tau = \hat{F}_n^{-1}(\tau) = X_{(\lceil n\tau \rceil)}$ satisfies the above inequality, it is a minimizer. If additionally $X_{(\lceil n\tau \rceil)} < X_{(\lceil n\tau \rceil+1)}$, then the inequality pins down a single point, hence the minimizer is unique and equals \hat{X}_τ . \square

In addition, the sample quantile is guaranteed to converge to the true quantile as n approaches infinity. It is guaranteed by the following theorem.

Theorem C.2 (Consistency of the sample quantile). *Let X be a real-valued random variable with cumulative distribution function F , and let*

$$X_\tau := F^{-1}(\tau) = \inf\{x \in \mathbb{R} : F(x) \geq \tau\}, \quad \tau \in (0, 1),$$

denote the population τ -quantile. Let \hat{F}_n be the sample distribution function based on i.i.d. samples $\{X_i\}_{i=1}^n$, and define the sample τ -quantile by

$$\hat{X}_\tau := \hat{F}_n^{-1}(\tau).$$

Assume that X_τ is unique, i.e., F is strictly increasing in a neighborhood of x_τ , and that F is continuous at X_τ . Then

$$\hat{X}_\tau \xrightarrow{a.s.} X_\tau \quad \text{as } n \rightarrow \infty.$$

Proof. By the Glivenko–Cantelli theorem, the sample distribution function \hat{F}_n converges uniformly to F almost surely. Since F is continuous and strictly increasing in a neighborhood of x_τ , the generalized inverse mapping F^{-1} is continuous at τ . The almost sure convergence $\hat{X}_\tau \rightarrow X_\tau$ then follows from the continuous mapping theorem. A detailed proof can be found in (Van der Vaart, 2000, p. 266). \square

Asymptotic Normality of the Sample Quantile. We now establish the asymptotic distribution of the empirical quantile \hat{X}_τ .

Theorem C.3 (Asymptotic normality of the sample quantile). *Let X_1, X_2, \dots, X_n be i.i.d. random variables with cumulative distribution function F and probability density function f . Fix $\tau \in (0, 1)$ and denote the population τ -quantile by $X_\tau = F^{-1}(\tau)$ and the empirical τ -quantile by $\hat{X}_\tau = \hat{F}_n^{-1}(\tau)$. If f is continuous at X_τ and $f(X_\tau) > 0$, then*

$$\sqrt{n}(\hat{X}_\tau - X_\tau) \xrightarrow{d} \mathcal{N}\left(0, \frac{\tau(1-\tau)}{f^2(X_\tau)}\right), \quad n \rightarrow \infty. \quad (26)$$

Proof. For any $t \in \mathbb{R}$, the event $\{\sqrt{n}(\hat{X}_\tau - X_\tau) \leq t\}$ is equivalent to $\hat{F}_n(X_\tau + t/\sqrt{n}) \geq \tau$. Hence

$$P\left(\sqrt{n}(\hat{X}_\tau - X_\tau) \leq t\right) = P\left(\hat{F}_n(X_\tau + t/\sqrt{n}) \geq \tau\right). \quad (27)$$

Introduce the decomposition

$$\sqrt{n}[\hat{F}_n(X_\tau + t/\sqrt{n}) - \tau] = A_n + B_n, \quad (28)$$

where

$$\begin{aligned} A_n &= \sqrt{n}[\hat{F}_n(X_\tau + t/\sqrt{n}) - F(X_\tau + t/\sqrt{n})], \\ B_n &= \sqrt{n}[F(X_\tau + t/\sqrt{n}) - \tau]. \end{aligned} \quad (29)$$

We analyze A_n and B_n separately.

For B_n , we expand F around X_τ and using $F(X_\tau) = \tau$ and obtain

$$B_n = f(X_\tau)t + o(1), \quad n \rightarrow \infty. \quad (30)$$

For A_n , we define $Y_{n,i} = \mathbb{I}(X_i \leq X_\tau + t/\sqrt{n})$ for $i = 1, \dots, n$. Then $\{Y_{n,i}\}$ are i.i.d. Bernoulli random variables with

$$\begin{aligned} \mathbb{E}[Y_{n,i}] &= F(X_\tau + t/\sqrt{n}), \\ \text{Var}(Y_{n,i}) &= F(X_\tau + t/\sqrt{n})[1 - F(X_\tau + t/\sqrt{n})]. \end{aligned} \quad (31)$$

It is straightforward to verify that

$$\lim_{n \rightarrow \infty} \mathbb{E}[Y_{n,i}] = \tau, \quad \lim_{n \rightarrow \infty} \text{Var}(Y_{n,i}) = \tau(1 - \tau). \quad (32)$$

Applying the Lindeberg–Feller central limit theorem yields

$$A_n = \sqrt{n} \left(\frac{1}{n} \sum_{i=1}^n Y_{n,i} - F(X_\tau + t/\sqrt{n}) \right) \xrightarrow{d} \mathcal{N}(0, \tau(1-\tau)). \quad (33)$$

Now, combining the two terms and according to Slutsky's theorem, we have that

$$A_n + B_n \xrightarrow{d} \mathcal{N}(f(X_\tau)t, \tau(1-\tau)). \quad (34)$$

Consequently,

$$\begin{aligned} \lim_{n \rightarrow \infty} P\left(\sqrt{n}(\hat{X}_\tau - X_\tau) \leq t\right) &= \lim_{n \rightarrow \infty} P(A_n + B_n \geq 0) \\ &= \Phi\left(\frac{f(X_\tau)t}{\sqrt{\tau(1-\tau)}}\right), \end{aligned} \quad (35)$$

where Φ denotes the standard normal distribution function. This shows that the limiting distribution of $\sqrt{n}(\hat{X}_\tau - X_\tau)$ is $\mathcal{N}(0, \tau(1-\tau)/f^2(X_\tau))$, completing the proof. \square

Bias of the Sample Quantile. Before presenting the formal result, we remark that no universally unbiased estimator exists for quantiles; we can only provide asymptotic statements. For a detailed discussion of this point, see (Lehmann & Casella, 1998, p. 84).

Theorem C.4 (Asymptotic bias of the sample quantile). *Let X_1, X_2, \dots, X_n be i.i.d. random variables with cumulative distribution function F and quantile function $Q(\tau) = F^{-1}(\tau)$. Fix $\delta > 0$ and consider $\tau \in [\delta, 1-\delta]$. Assume that:*

- (i) *The density f satisfies $\inf_{\tau \in [\delta, 1-\delta]} f(Q(\tau)) \geq c > 0$ for some constant c ;*
- (ii) *Q is differentiable on $[\delta, 1-\delta]$;*
- (iii) *$\mathbb{E}[X^2] < \infty$.*

Then the bias of the empirical quantile $\hat{Q}_n(\tau) = \hat{X}_\tau$ satisfies

$$|\mathbb{E}[\hat{Q}_n(\tau)] - Q(\tau)| = o\left(\frac{1}{\sqrt{n}}\right). \quad (36)$$

Proof. Write $U_i = F(X_i) \sim \text{Uniform}(0, 1)$ and let $U_{(1)} \leq \dots \leq U_{(n)}$ be the order statistics. Set $k = \lceil n\tau \rceil$ and $V_n = U_{(k)} - \tau$. Then $\hat{Q}_n(\tau) = Q(U_{(k)}) = Q(\tau + V_n)$.

A first-order Taylor expansion yields

$$\hat{Q}_n(\tau) - Q(\tau) = Q'(\tau)V_n + r(V_n), \quad (37)$$

where the remainder $r(v)$ satisfies the Peano form: for every $\epsilon > 0$ there exists $\delta_\epsilon > 0$ such that $|r(v)| \leq \epsilon|v|$ whenever $|v| \leq \delta_\epsilon$.

From properties of the Beta distribution,

$$\mathbb{E}[V_n] = \frac{k}{n+1} - \tau, \quad \text{Var}(V_n) = \frac{\tau(1-\tau)}{n} + O\left(\frac{1}{n^2}\right). \quad (38)$$

By Jensen's inequality,

$$\mathbb{E}[|V_n|] \leq \sqrt{\mathbb{E}[V_n^2]} = \sqrt{\text{Var}(V_n) + (\mathbb{E}[V_n])^2} = O\left(\frac{1}{\sqrt{n}}\right). \quad (39)$$

To bound $\mathbb{E}[|r(V_n)|]$, we first estimate the second moment of $r(V_n)$. Using the elementary inequality $(a+b+c)^2 \leq 3(a^2 + b^2 + c^2)$,

$$\begin{aligned} r(V_n)^2 &= (Q(\tau + V_n) - Q(\tau) - Q'(\tau)V_n)^2 \\ &\leq 3\left(Q^2(\tau + V_n) + Q^2(\tau) + (Q'(\tau))^2V_n^2\right). \end{aligned} \quad (40)$$

Hence

$$\mathbb{E}[r(V_n)^2] \leq 3 \left(\mathbb{E}[X_{(k)}^2] + Q^2(\tau) + (Q'(\tau))^2 \mathbb{E}[V_n^2] \right), \quad (41)$$

where $X_{(k)} = Q(U_{(k)})$ is the k -th order statistic of the original sample. Because $\mathbb{E}[X^2] < \infty$, there exists a constant $A > 0$ such that $\mathbb{E}[r(V_n)^2] \leq An$.

Next, the Dvoretzky–Kiefer–Wolfowitz inequality gives

$$P(|V_n| \geq t) \leq 2 \exp(-2nt^2), \quad t > 0. \quad (42)$$

Split the expectation of $|r(V_n)|$ into two parts. For a given $\epsilon > 0$, take the corresponding δ_ϵ :

$$\begin{aligned} \mathbb{E}[|r(V_n)|] &= \mathbb{E}\left[|r(V_n)| \mathbb{I}\{|V_n| \leq \delta_\epsilon\}\right] + \mathbb{E}\left[|r(V_n)| \mathbb{I}\{|V_n| > \delta_\epsilon\}\right] \\ &\leq \epsilon \mathbb{E}[|V_n|] + \sqrt{\mathbb{E}[r(V_n)^2]} \sqrt{P(|V_n| > \delta_\epsilon)} \\ &\leq \epsilon O\left(\frac{1}{\sqrt{n}}\right) + \sqrt{An} \sqrt{2 \exp(-2n\delta_\epsilon^2)} \\ &= \epsilon O\left(\frac{1}{\sqrt{n}}\right) + o\left(\frac{1}{\sqrt{n}}\right). \end{aligned} \quad (43)$$

Since $\epsilon > 0$ is arbitrary, we obtain

$$\mathbb{E}[|r(V_n)|] = o\left(\frac{1}{\sqrt{n}}\right). \quad (44)$$

Finally, combining (37), (39) and (44),

$$\begin{aligned} |\mathbb{E}[\hat{Q}_n(\tau)] - Q(\tau)| &\leq |Q'(\tau)| |\mathbb{E}[V_n]| + \mathbb{E}[|r(V_n)|] \\ &\leq \frac{1}{c} \cdot \frac{1}{n+1} + o\left(\frac{1}{\sqrt{n}}\right) \\ &= o\left(\frac{1}{\sqrt{n}}\right), \end{aligned} \quad (45)$$

which completes the proof. \square

Accordingly, letting $n = K_{\text{tgt}}$, we show that, given K_{tgt} target samples, the resulting asymptotic bias is $o(1/\sqrt{K_{\text{tgt}}})$.

Remark. The assumption $\inf_{\tau \in [\delta, 1-\delta]} f(Q(\tau)) \geq c > 0$ guarantees that $Q'(\tau) = 1/f(Q(\tau))$ is bounded on $[\delta, 1-\delta]$. If one further assumes that Q' satisfies Lipschitz Condition, a sharper $O(1/n)$ bias bound can be derived. Restricting to the inner interval $[\delta, 1-\delta]$ covers the quantile levels that are most relevant in practice while providing the necessary regularity for the analysis.

D. Full Algorithm

Here, the *generator* corresponds to a specific instantiation of Eq. (4) under a predefined scheduling scheme.

Algorithm 3 GOU-BQC: Training and Inference

- 1: **Inputs:** replay buffer \mathcal{D} ; online parameters θ ; target parameters ϕ
- 2: **Hyperparameters:** heads H ; discount γ ; temperature α ; target atoms K_{target} ; online atoms K ; time steps T ; TQC drop d ; max updates N_{step} ; EMA coefficient τ_{tgt} ; Generator
- 3: **Notation:** $m \in \{0, 1\}$ is the terminal mask; $\text{sac} = \alpha \log \pi(\mathbf{a}' \mid \mathbf{s}')$
- 4: **Part I: Training (performed for N_{step} updates)**
- 5: $i \leftarrow 0$
- 6: **while** $i < N_{\text{step}}$ **do**
- 7: $i \leftarrow i + 1$
- 8: Sample $(\mathbf{s}, \mathbf{a}, r, \mathbf{s}', m) \sim \mathcal{D}$
- 9: **(A) Target atoms (no gradient).**
- 10: Sample $\tau' \sim U([0, 1]^{K_{\text{target}}})$ and set $z'^{\text{start}} \leftarrow \tau'$
- 11: $\{z_{\text{target}}^{(h)}\}_{h=1}^H \leftarrow \text{Generator}(z'^{\text{start}}, \mathbf{s}', \mathbf{a}', \tau', \phi)$
- 12: Stack atoms $Z \leftarrow \text{Concat}(z_{\text{target}}^{(1)}, \dots, z_{\text{target}}^{(H)})$
- 13: Apply truncation $Z_{\text{tqc}} \leftarrow \text{DropTop}(Z, d \cdot H)$
- 14: Build target samples $y_{\text{target}} \leftarrow r + m\gamma(Z_{\text{tqc}} - \text{sac})$
- 15: **(B) Online samples and empirical quantiles.**
- 16: Sample $\tau \sim U([0, 1]^K)$ and set $z^{\text{start}} \leftarrow \tau$
- 17: $\hat{z}_\tau \leftarrow \text{SampleQuantile}(y_{\text{target}}, \tau)$
- 18: **(C) Online predictions at $t = 0$ and $t = t_m$.**
- 19: Sample $t_m \sim \text{Unif}(0, 1)$
- 20: $z_{t_m} \leftarrow \xi(t_m) \hat{z}^{\text{end}} + (1 - \xi(t_m)) z^{\text{start}}$
- 21: **for** $h = 1$ **to** H **do**
- 22: $\hat{z}_{\tau,0}^{(h)} \leftarrow f_{\theta,h}(z^{\text{start}}, \mathbf{s}, \mathbf{a}, \tau, 0)$
- 23: $\hat{z}_{\tau,m}^{(h)} \leftarrow f_{\theta,h}(z_{t_m}, \mathbf{s}, \mathbf{a}, \tau, t_m)$
- 24: $\mathcal{L}^{(h)} \leftarrow \mathcal{L}\left(\hat{z}_{\tau,0}^{(h)}, \hat{z}_{\tau,m}^{(h)}; \hat{z}_\tau, z^{\text{start}}, t_m\right)$ by Eq. (12).
- 25: **end for**
- 26: **(D) Loss and updates.**
- 27: $\mathcal{L}_{\text{total}} \leftarrow \frac{1}{H} \sum_{h=1}^H \mathcal{L}^{(h)}$
- 28: Update θ by descending $\nabla_\theta \mathcal{L}_{\text{total}}$
- 29: Soft-update target parameters $\phi \leftarrow \tau_{\text{tgt}}\phi + (1 - \tau_{\text{tgt}})\phi$
- 30: **end while**
- 31: **Part II: Inference (Q-value evaluation)**
- 32: **Input:** a state-action pair (\mathbf{s}, \mathbf{a})
- 33: Sample $\tau \sim U([0, 1]^K)$ and set $z^{\text{start}} \leftarrow \tau$
- 34: $\{z^{(h)}\}_{h=1}^H \leftarrow \text{Generator}(z^{\text{start}}, \mathbf{s}, \mathbf{a}, \tau, \theta)$
- 35: Stack atoms $Z \leftarrow \text{Concat}(z^{(1)}, \dots, z^{(H)})$
- 36: Output $Q(\mathbf{s}, \mathbf{a}) \leftarrow \text{Mean}(Z)$

E. Baseline Methods and Implementation Details

Here we provide additional details on the baseline methods reported in Table 1 of the main paper. We summarize their distributional assumptions and generative mechanisms, and clarify the implementation and comparison protocols adopted in our experiments.

TD3 (Fujimoto et al., 2018). CDQ (Clipped Double Q-Learning), originally introduced in TD3, models the critic as a scalar-valued function and mitigates overestimation by taking the minimum over multiple Q-value estimates. It does not explicitly maintain a return distribution and thus corresponds to a non-distributional critic with an implicit point-mass

assumption. The official torch implementation for TD3 is available at:

<https://github.com/sfujim/TD3>

SAC (Haarnoja et al., 2018). SAC (Soft Actor-Critic) is an off-policy actor-critic algorithm that learns a stochastic policy under the maximum-entropy reinforcement learning framework. By explicitly encouraging policy entropy during training, SAC improves exploration and robustness while maintaining strong sample efficiency. In practice, SAC maintains a pair of Q-functions and uses a clipped double-Q target to mitigate overestimation. It also supports automatic temperature adjustment, which adapts the strength of the entropy regularization to match a target entropy. We implement SAC in our unified codebase and use it as the default actor backbone in our experiments. The official tensorflow implementation for SAC is available at:

<https://github.com/haarnoja/sac>

QVPO (Ding et al., 2024). QVPO (Q-weighted Variational Policy Optimization) is an online diffusion-policy reinforcement learning algorithm that parameterizes the actor as a conditional diffusion model, thereby capturing multimodal action distributions. To bridge diffusion-model training with online policy optimization, QVPO introduces a Q-weighted variational objective that re-weights the diffusion training signal using value estimates and further employs a weight transformation to handle general settings where raw Q-values may not be strictly positive. In addition, QVPO incorporates a tailored entropy regularization to encourage exploration and proposes an efficient behavior/action selection strategy to reduce the variance of diffusion-policy rollouts during online interaction. We follow the official implementation and integrate it into our unified framework:

<https://github.com/wadx2019/qvpo>.

DSAC (Duan et al., 2022). DSAC models the return distribution as a Gaussian distribution, parameterized by a learned mean and variance. Under this assumption, the entire return distribution can be represented compactly, and target sampling reduces to sampling from a Gaussian. We base our implementation on the official DSAC codebase:

<https://github.com/Jingliang-Duan/DSAC-v2>.

Specifically, we integrate the DSAC-v1 implementation into our unified code framework and use it as the DSAC baseline.

IQN (Dabney et al., 2018a). IQN explicitly models the continuous quantile function of the return distribution. Quantile levels are embedded using cosine features, which improves the representation of high-frequency distributional structures. We implement IQN following the original paper. When combined with a SAC actor, IQN can be viewed as a particular instantiation of the DSAC (Ma et al., 2025b) framework, where DSAC here denotes the general distributional SAC formulation rather than the Gaussian-based DSAC baseline discussed earlier.

TQC (Kuznetsov et al., 2020). TQC extends quantile-based critics by aggregating multiple critic heads and truncating the highest quantile estimates (Drop-Top) to control overestimation. Compared to CDQ, which may introduce systematic underestimation by taking a hard minimum, TQC provides a finer-grained and more robust control mechanism. Our implementation is adapted from the official PyTorch reference:

https://github.com/alxlampe/tqc_pytorch.

and integrated into our unified framework.

VF (Dong et al., 2025). Value Flows (VF) combine Flow Matching with distributional critics and primarily target offline reinforcement learning. The original implementation is written in JAX and available at:

<https://github.com/chongyi-zheng/value-flows>.

We re-implement the method in PyTorch based on the official code and extract only the critic component for comparison, decoupling it from the original actor design.

Table 6. Comparison of baseline methods by distributional assumption and generative mechanism.

Method	Distribution Assumption	Representation	Generative Mechanism	Aggregation
CDQ	Point mass	Scalar $Q(s, a)$	Deterministic evaluation	Min
DSAC	Gaussian	(μ, σ)	Gaussian sampling	Mean
IQN	Quantile	$F^{-1}(\tau)$	Quantile sampling	Mean/Min
TQC	Quantile	$F^{-1}(\tau_i)$	Quantile sampling	Drop-Top
VF	Flow	Velocity field	Flow-based sampling	Mean/Min
VDRL	Diffusion	noise predictor	Reverse diffusion	Mean/Min
DBC (Ours)	Diffusion Bridge	End Point $\hat{x}_1(\tau, t)$	ODE bridge sampling	Drop-Top

VDRL (Hu et al., 2025). VDRL (Value Diffusion Reinforcement Learning) models the return distribution using diffusion models and is designed for online reinforcement learning. At the time of submission, no official implementation is publicly available. We implement VDRL from scratch based on the descriptions in the original paper and integrate it into our unified framework as a baseline.

Implementation and comparison protocol. To ensure a fair and consistent comparison across baselines, we adopt the following unified design principles:

- **Implementation source.** For methods with official implementations (e.g., DSAC, TQC, VF), we base our implementations on the official code. For methods originally implemented in JAX (e.g., VF), we provide corresponding PyTorch re-implementations. All baselines are integrated into the same unified code framework.
- **Actor-critic decoupling.** For all baselines, we decouple the critic from the actor and evaluate only the critic component under a unified training and evaluation pipeline.
- **Target construction.** For entropy-regularized methods, target return samples are constructed as

$$r + \gamma(Z^{\text{tgt}}(s', a') - \alpha \log \pi(a' | s')).$$

For non-entropy-based methods, target return samples are constructed as

$$r + \gamma Z^{\text{tgt}}(s', a').$$

- **Distributional aggregation.** For critics with multiple heads or multiple return distributions, we consider the following aggregation schemes:

1. Mean aggregation:

$$\frac{1}{H} \sum_{h=1}^H \mathbb{E}[Z_h].$$

2. Min aggregation:

$$\mathbb{E}[\min_h Z_h].$$

3. Drop-Top aggregation (TQC): truncating the largest quantile estimates before computing expectations.

These design choices ensure that all baselines are evaluated under consistent training signals and target semantics, isolating the effects of different distributional assumptions and generative mechanisms. We provide a concise summary of these methods in Table 6 to facilitate a clear comparison and highlight the key differences among them.

F. Detailed Experimental Settings

In this section, we briefly describe the hyperparameters used for each baseline in our experiments. Since our codebase adopts a fully decoupled design for the actor and the critic, we present their hyperparameters separately. Specifically, we report the settings for the actor algorithms, QVPO, SAC, and TD3, as well as for the critic algorithms, DSAC, IQN, DBC, TQC, CDQ, VF, and VD. A detailed summary of the actor hyperparameters is provided in Table 7.

Table 7. Actor-side hyperparameters for QVPO, SAC, and TD3. Here, “–” indicates that the corresponding actor does not involve this hyperparameter.

Parameter	QVPO	SAC	TD3
<i>Base Settings</i>			
Discount factor γ	0.99	0.99	0.99
Target update rate τ	0.005	0.005	0.005
<i>Actor Network Architecture</i>			
Hidden units	256	256	256
Time embedding dim	32	–	–
Hidden layers	3	3	3
Activation layer	Mish	ReLU	ReLU
<i>Diffusion Parameterization</i>			
Number of diffusion steps T	20	–	–
Beta schedule	Cosine	–	–
Predict noise ϵ	True	–	–
Noise ratio	1.0	–	–
<i>Optimization (Actor Only)</i>			
Actor learning rate	1×10^{-4}	3×10^{-4}	3×10^{-4}
Gradient clipping	2.0	1.0	1.0
<i>Sampling / Policy Evaluation</i>			
Train samples per state	64	–	–
Eval samples per state	32	–	–
<i>Regularization / Entropy</i>			
Entropy coefficient α	0.02	1	–
Minimum α	0.002	–	–
<i>Update Frequency</i>			
Policy Delay	1	1	2

Due to the nature of distributional reinforcement learning, the sampling and aggregation schemes of distributional critics are an important part of the experimental configuration and thus are reported separately in Table 9. In this table, we only specify the aggregation mode for combining the outputs of heads; by default, the final critic output is obtained by averaging over samples (i.e. $\frac{1}{n} \sum_{i=1}^n z_i$). DSAC is excluded from Table 9 because it models the return distribution as a Gaussian and directly predicts the return mean (and variance), rather than relying on multi-sample estimation and aggregation as in other distributional methods.

Table 8. Common critic hyperparameters across methods.

Parameter	DSAC-V1	IQN	DBC	TQC	CDQ	ValueFlows	VDRL
Network Structure	MLP	IQN	MLP	MLP	MLP	MLP	MLP
Hidden width	256	256	512	512	512	512	256
Activation	GELU	ReLU	ReLU	ReLU	ReLU	ReLU	Mish
Number of heads	1	2	2	2	2	2	2
Optimizer	Adam						
Learning rate	3×10^{-4}						
Adam ϵ	10^{-5}	10^{-5}	10^{-5}	10^{-5}	10^{-5}	10^{-5}	10^{-8}
Gradient clip (max norm)	1.0	1.0	1.0	1.0	1.0	1.0	1.0
Discount γ	0.99	0.99	0.99	0.99	0.99	0.99	0.99
Target Polyak τ	0.005	0.005	0.005	0.005	0.005	0.005	0.005

Table 10 presents the configurations for DBC and TQC, which are the two algorithms adopting the DropTop aggregation scheme. Notably, our TQC’s setting strictly adheres to the settings reported in its original paper.

Table 9. Comparison of online/target sampling counts and aggregation strategies. IQN aggregates via minimum over sampled quantiles; TQC and DBC apply top value truncation, with DBC using asymmetric online/target sampling. Here, “-” indicates that the corresponding critic does not involve this hyperparameter.

Method	Aggregation	Online Samples	Target Samples	Embedding Dimension
VF	Mean	1	1	1
VDRL	Min	5	10	16
IQN	Min	32	32	64
TQC	Drop-top	25	25	—
DBC	Drop-top	64	128	32

Table 10. Drop ratios for DBC and TQC across environments. TQC drop settings strictly follow the original TQC paper, while DBC uses environment-specific truncation ratios under a higher-resolution target distribution.

Environment	DBC (Drop / Total)	TQC (Drop / Total)
HalfCheetah-v5	0/128	0/25
Ant-v5	12/128	2/25
Walker2d-v5	14/128	2/25
Humanoid-v5	12/128	2/25
Hopper-v5	32/128	5/25

G. Full Experiments

Experimental Environment. All experiments were conducted on a Linux server running Ubuntu 22.04.5 LTS with kernel version 5.15.0. The machine is equipped with two Intel Xeon Platinum 8480+ CPUs, providing 224 logical cores in total and 2 TiB of system memory. For acceleration, we use 8 NVIDIA H20 GPUs, each with 96 GB of HBM memory, driven by NVIDIA driver 580.95.05. The software stack consists of Python 3.12.12 and PyTorch 2.9.1 compiled with CUDA 12.8, with CUDA runtime support verified during execution. Unless otherwise stated, all reported results are obtained under this hardware and software configuration.

Throughout this section, unless stated otherwise, we adopt the following default hyperparameters: $M = 5$, $w = 0.01$, and $\theta_t = 1$.

G.1. Detailed Results for All Baselines

Table 11. Experiments Performance for all baselines

Run	Ant-v5	HalfCheetah-v5	Hopper-v5	Humanoid-v5	Walker2d-v5
QVPO+CDQ	6373.2 ± 65.0	12103.9 ± 422.3	3582.0 ± 48.1	5068.3 ± 28.5	4986.3 ± 279.6
SAC+CDQ	6121.8 ± 412.7	12776.4 ± 285.2	3630.5 ± 50.0	5207.1 ± 94.1	4854.4 ± 372.8
SAC+DSAC	2013.2 ± 679.9	12974.0 ± 191.7	3522.9 ± 23.5	3442.6 ± 216.8	3297.4 ± 1248.3
SAC+IQN	3487.4 ± 798.5	10930.2 ± 152.7	3301.8 ± 360.1	4729.2 ± 580.5	4766.5 ± 255.7
SAC+TQC	6342.6 ± 294.7	13996.2 ± 191.7	3704.6 ± 94.5	5269.0 ± 113.8	5802.6 ± 234.2
SAC+VD	3850.4 ± 987.1	4284.8 ± 478.2	1052.7 ± 20.4	4886.9 ± 228.8	2533.9 ± 302.4
SAC+VF	2650.3 ± 163.8	8199.5 ± 1533.3	3310.4 ± 24.6	4950.3 ± 60.3	2626.4 ± 1387.4
TD3+CDQ	4257.0 ± 1711.6	11679.0 ± 629.8	3596.2 ± 38.8	5067.8 ± 33.7	5093.7 ± 439.8
SAC+DBC(*)	6501.4 ± 84.3	13120.2 ± 162.4	3732.5 ± 83.2	5906.7 ± 198.6	6138.2 ± 38.1
QVPO+DBC(*)	6633.8 ± 71.2	13182.1 ± 252.4	3721.3 ± 116.6	5426.3 ± 9.0	5448.1 ± 193.8
TD3+DBC(*)	5306.0 ± 1303.6	13787.8 ± 346.5	3685.7 ± 68.2	5343.2 ± 199.3	6335.5 ± 269.4

G.2. Ablation for Different Schedules

We observe that the constant and linear schedules exhibit comparable performance, whereas the cosine schedule results in substantially higher variance. Therefore, for the case of $M = 5$, we recommend using either the constant or the linear schedule.

G.3. Ablation for Different Weights

We further investigate the effect of different values of the weight w across a wider range of tasks. Empirical results show that a small weight w (e.g., 0.01 or 0.02) consistently leads to performance improvements. However, as w increases, the

Table 12. Ablation for different schedules

Schedule	Ant-v5	HalfCheetah-v5	Hopper-v5	Humanoid-v5	Walker2d-v5
Constant	6501.4 ± 84.3	13120.2 ± 162.4	3732.5 ± 83.2	5906.7 ± 198.6	6138.2 ± 38.1
Cosine	5358.3 ± 1628.9	12538.9 ± 266.1	3748.6 ± 144.4	5623.8 ± 368.7	6326.6 ± 751.9
Linear	6544.5 ± 113.9	13004.6 ± 174.7	3728.6 ± 50.9	5594.4 ± 305.7	6116.7 ± 517.3

performance may begin to deteriorate. For reference, when training is performed solely with the Anchor Loss, the resulting performance is generally poor. This indicates that the Anchor Loss should not be used in isolation, but rather as a weak auxiliary loss to facilitate convergence. Based on these observations, we recommend setting $w = 0.01$.

 Table 13. Sensitivity Analysis of Anchor Loss Weight w

	Ant-v5	HalfCheetah-v5	Hopper-v5	Humanoid-v5	Walker2d-v5
$w = 0.0$	4828.3 ± 1439.0	12990.1 ± 719.7	3646.3 ± 84.9	5807.3 ± 175.8	5562.9 ± 423.2
$w = 0.01$	6501.4 ± 84.3	13120.2 ± 162.4	3748.6 ± 144.0	5906.7 ± 198.6	6138.2 ± 38.1
$w = 0.02$	3947.3 ± 2151.8	13165.8 ± 301.2	3702.6 ± 86.5	5743.4 ± 301.1	6097.8 ± 375.1
$w = 0.1$	5716.2 ± 741.3	12775.5 ± 127.8	3591.1 ± 79.2	5589.0 ± 50.3	5974.6 ± 603.2
No Eq. (8)	2517.1 ± 2464.7	12393.1 ± 314.9	3244.0 ± 497.5	3751.2 ± 321.1	3859.3 ± 1828.7

G.4. Ablation for Different Time Steps

We further examine the impact of the number of flow steps (M) across a wider range of tasks. Consistent with the results in the main text, we find that ($M = 5$) yields the best overall performance.

 Table 14. Ablation of Flow Steps M

	Ant-v5	HalfCheetah-v5	Hopper-v5	Humanoid-v5	Walker2d-v5
M=1	5150.4 ± 2226.3	12821.5 ± 26.4	3748.1 ± 46.8	5524.7 ± 132.7	5809.8 ± 308.6
M=5	6501.4 ± 84.3	13120.2 ± 162.4	3748.6 ± 144.4	5906.7 ± 198.6	6138.2 ± 38.1
M=10	5946.6 ± 379.7	13066.6 ± 203.0	3607.9 ± 30.5	4848.7 ± 88.1	6014.3 ± 561.6

G.5. Training Time Across Benchmarks

As shown in Table 15, although DBC employs a multi-step reward generation process in the critic, the resulting training-time overhead remains manageable. Compared to other baselines, DBC incurs only an approximately 2 increase in training time.

Table 15. Training time (in hours) required by different critics to complete 1M environment steps. All experiments use SAC as the actor backbone and are evaluated on MuJoCo v5 benchmarks.

Critic	Ant-v5	HalfCheetah-v5	Hopper-v5	Walker2d-v5	Humanoid-v5
CDQ	3.0	3.0	3.0	3.0	3.5
TQC	3.1	3.0	3.3	3.3	3.5
IQN	4.0	4.0	4.0	4.0	3.8
DBC	7.0	7.0	7.0	7.0	8.0